Available online at www.sciencedirect.com

ScienceDirect

www.elsevier.com/locate/jes

JES JOURNAL OF ENVIRONMENTAL SCIENCES

www.jesc.ac.cn

Characterization of a new smog chamber for evaluating SAPRC gas-phase chemical mechanism

Kangwei Li[1,2,3,*], *Chao Lin*[2], *Chunmei Geng*[1], *Stephen White*[4], *Linghong Chen*[2], *Zhier Bao*[2], *Xin Zhang*[2], *Yanyun Zhao*[2], *Lixia Han*[2], *Wen Yang*[1,*], *Merched Azzi*[3]

[1] *State Key Laboratory of Environmental Criteria and Risk Assessment, Chinese Research Academy of Environmental Sciences, Beijing 100012, China*

[2] *State Key Laboratory of Clean Energy Utilization, Zhejiang University, Hangzhou 310027, China*

[3] *CSIRO Energy, North Ryde, NSW 1670, Australia*

[4] *New South Wales Department of Planning, Industry and Environment, Lidcombe, NSW 1825, Australia*

ARTICLE INFO

Article history:
Received 29 September 2019
Revised 6 February 2020
Accepted 17 March 2020
Available online 7 May 2020

Keywords:
Smog chamber
Chemical mechanism
Chamber characterization
SAPRC
Ozone

ABSTRACT

A new state-of-the-art indoor smog chamber facility (CAPS-ZJU) has been constructed and characterized at Zhejiang University, which is designed for chemical mechanism evaluation under well-controlled conditions. A series of characterization experiments were performed to validate the well-established experimental protocols, including temperature variation pattern, light spectrum and equivalent intensity (J_{NO2}), injection and mixing performance, as well as gases and particle wall loss. In addition, based on some characterization experiments, the auxiliary wall mechanism has been setup and examined. Fifty chamber experiments were performed across a broad range of experimental scenarios, and we demonstrated the ability to utilize these chamber data for evaluating SAPRC chemical mechanism. It was found that the SAPRC-11 can well predict the O_3 formation and NO oxidation for almost all propene runs, with 6 hr $\Delta(O_3 - NO)$ model error of –3% ± 7%, while the final O_3 was underestimated by ~20% for isoprene experiments. As for toluene and *p*-xylene experiments, it was confirmed that SAPRC-11 has significant improvement on aromatic chemistry than earlier version of SAPRC-07, although the aromatic decay rate was still underestimated to some extent. The model sensitivity test has been carried out, and the most sensitive parameters identified are the initial concentrations of reactants and the light intensity as well as HONO offgasing rate and O_3 wall loss rate. All of which demonstrated that CAPS-ZJU smog chamber could derive high quality experimental data, and could provide insights on chamber studies and chemical mechanism development.

Introduction

Air pollution is one of the most challenging environmental issues in the world, and a better understanding of atmospheric chemistry can provide great benefits to human health, climate change and ecological systems (Seinfeld and Pandis, 2016). It has been well recognized that the chemical reactions are extremely complex in the real atmosphere, given the continuous changes of emissions and meteorology. The smog chamber (or simulation chamber) has the advantage to isolate atmospheric chemistry for a few selected compounds under well-

* Corresponding authors.
E-mails: likangweizju@foxmail.com (K. Li), yangwen@craes.org.cn (W. Yang).

https://doi.org/10.1016/j.jes.2020.03.028
1001-0742/

controlled conditions (Hidy, 2019). Therefore, for the past few decades, a great number of smog chambers have been constructed worldwide and are being used for various purposes, in particular for gas-phase chemistry (Bloss et al., 2005; Hess et al., 1992; Hynes et al., 2005) and secondary organic aerosol (SOA) formation mechanism (Boyd et al., 2015; Hildebrandt et al., 2009; Ng et al., 2007). These laboratory chamber studies have largely improved our fundamental understanding on atmospheric chemistry, and provide scientific support for air pollution control strategy and policy planning.

The chemical mechanism is the core of the chemical transport models (CTMs), which representing chemical reactions for emitted pollutants to form secondary pollutants. There are a variety of chemical mechanisms being utilized in CTMs, including CB05 (Yarwood et al., 2005), CB6 (Yarwood et al., 2010), RACM (Goliff et al., 2013; Stockwell et al., 1997), SAPRC-07 (Carter, 2010), and MECCA 3.0 (Bonn et al., 2018). Unlike explicit chemistry (e.g., Master Chemical Mechanism (MCM)), these mechanisms are treated in lumping way for simplicity, as limited number of reactions and species are required and applicable for CTM runs. Each of these mechanisms includes reactions within forming and propagating peroxy radicals (HO_2 and RO_2), but they are different in the detail and describing the precursor VOC (volatile organic compound) chemistry.

One major consideration for chamber studies is to evaluate various chemical mechanisms against smog chamber data, which is regarded as the ability to utilize the experimental results to afford an improved understanding or prediction of the chemistry to the ambient atmosphere, in particular for latest version of chemical mechanisms. Smog chamber characterization is critical prior to further use in studying atmospheric chemistry and aerosol formation, as limitations or uncertainties in chamber wall effects are inevitable regardless of chamber volumes or types. For example, offgasing of NO_x and other species from chamber walls may introduce contaminations into the background gas and affect experiment results (Carter et al., 2005). Therefore, a detailed characterization of the chamber is needed to provide basic information and auxiliary wall mechanism for chemical mechanism evaluation.

There are a few versions of SAPRC series chemical mechanisms, such as SAPRC-99 (Carter, 2000), SAPRC-07 (Carter, 2010), SAPRC-11 (Carter and Heo, 2013), and SAPRC-16 (Venecek et al., 2018). The evolution of the SAPRC chemical mechanisms over the past 30 years reflects our expanding knowledge about atmospheric gas-phase chemistry (Venecek et al., 2018). Note that SAPRC-16 is still an interim version and under development, therefore this version is not yet available for the larger research community. SAPRC-11 has updated aromatic chemistry compared to previous version, which represents the current state of the science. However, SAPRC-11 has not yet integrated into commercialized chemical transport model (e.g., Community Multiscale Air Quality Modeling System (CMAQ)). To our best knowledge, only UCR (Carter and Heo, 2013) and CSIRO (White et al., 2018) chamber data have been used to evaluate the performance of SAPRC-11. Therefore, there is a potential research need to evaluate SAPRC-11 against new experimental data, in particular for the data derived from the well-characterized chambers, in order to overcome chamber-specific effects before SAPRC-11 being implemented into CTMs.

In this study, we described a new state-of-the-art indoor smog chamber facility (Complex Air Pollution Study-Zhejiang University, CAPS-ZJU), which was designed to evaluate current gas-phase chemical mechanisms and study aerosol formation. The CAPS-ZJU smog chamber has been characterized and discussed in detail, including temperature and relative humidity variation, light sources, injection and mixing, as well as chamber wall loss. The auxiliary wall mechanism for SAPRC has been setup and verified through some characterization

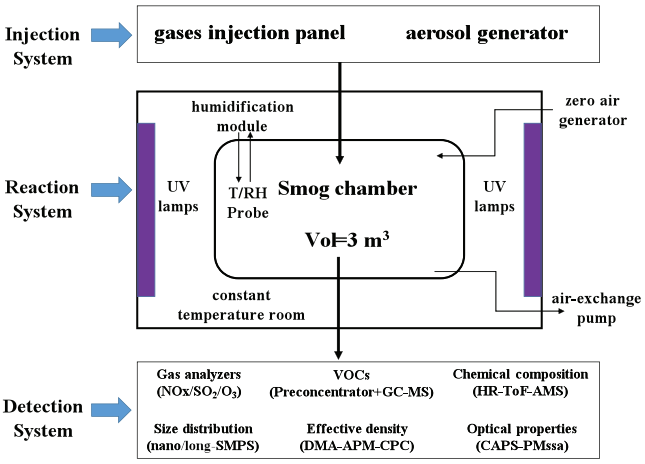

Fig. 1 – Schematic of the CAPS-ZJU smog chamber facility.

experiments. In addition, a large set of chamber experiments from propene, isoprene, toluene, and *p*-xylene in the presence of NO_x have been used to examine the performance of SAPRC chemical mechanism, and model sensitivity for input parameters has been tested as well. All of which could provide insights on chemical mechanism development, and also provide suggestions and guidance for the future chamber studies.

1. Materials and methods

1.1. *Chamber description*

The CAPS-ZJU (Complex Air Pollution Study-Zhejiang University) smog chamber facility has been originally constructed since end of 2015, and a few research related to aerosol formation have been carried out previously, including soot particle aging (Li et al., 2017a), new particle formation (Li et al., 2017b), and SOA formation (Chen et al., 2017). In the early 2018, we updated the facility including the replacement of the reactor, and established new experimental protocols for chamber runs, which was mostly followed from the well-organized procedures of CSIRO smog chamber (Li et al., 2018; White et al., 2018).

The schematic diagram of CAPS-ZJU smog chamber is shown in Fig. 1, which is consisted of injection system, reaction system and detection system. Injection system is consisted by gases injection panel and aerosol generators. Different kinds of gas pollutants and particle can be injected into the chamber according to experiment required. Reaction system is a 3 m^3 Teflon (fluorinated ethylene propylene, FEP) chamber located in a well-controlled enclosure, with 60 ultraviolet (UV) lamps surrounding. Detection system is consisted by a suite of state-of-the-art instruments, the chemical composition, mass concentration, size distribution, effective density and some other physicochemical properties of particles as well as gases concentration can be determined.

1.2. *Experiments summary*

A total of 50 experiments across a broad range of scenarios have been undertaken in the CAPS-ZJU smog chamber for SAPRC chemical mechanism evaluation, which are summarized in Appendix A Table S1. Specifically, 40 experiments using propene, 3 experiments were undertaken using isoprene, 4 for toluene and 3 for *p*-xylene. Propene was selected as it is a reactive species with a relatively simple degradation

mechanism, which is useful as the baseline and the starting point for mechanism modelling of chamber experiment. Isoprene and two aromatic hydrocarbons were chosen for their well-recognized importance from biogenic and anthropogenic emissions. It should be noted that experiments described in this work represent only dry conditions (relative humidity (RH) below 10%) and same temperature variation pattern, which do not represent the full range of environmental conditions in the real atmosphere.

Supplementary experiments were also performed for a variety of purposes, including CO-NO_x experiments, pure air experiments, photolysis test, as well as wall loss experiments, and these characterization experiments are summarized in Appendix A Table S2.

1.3. *Chemical mechanism model*

The SAPRC-11 mechanism was compiled into the existing SAPRC box model software used for chamber experiments, and this is available from SAPRC website (http://www.cert.ucr.edu/~carter/SAPRC/). The smog chamber experiments were simulated using this model with additional auxiliary wall mechanism, and the performance of the SAPRC-11 mechanism was compared against experiment data and also against earlier version of the SAPRC mechanism.

2. Results and discussion

2.1. *Chamber characterization*

2.1.1. *Temperature variation pattern*

Temperature is an important parameter through chamber experiment process, and it is usually affected by a few factors including room temperature, chamber air conditioning, and heat release after lights on, etc. An ideal chamber environment would have the ability to control temperature widely and precisely as required, however, only a few research groups in the world have equipped with advanced temperature control system with a wider range of temperature for chamber experiments. Currently, CAPS-ZJU chamber facility did not have this kind of equipment. Alternatively, we tried to maintain the room temperature constantly at ~20°C, and to make sure that the chamber temperature variation profile is similar and comparable for each experiment.

As shown in Appendix A Fig. S1, a short period was selected with temperature and humidity recording for both chamber and room environment. After UV lights on, the chamber temperature increased from ~20 to ~35°C quickly (within 2 hr) due to the lights heating, and then the chamber temperature maintained stable at ~35°C till the end of experiment. Note that the room temperature and relative humidity (RH) were maintained constantly at ~20 and 30%–40%, and the chamber RH was below 5% for the whole period. All the CAPS-ZJU chamber experiments have the similar temperature rising profile, which could make sure that the experiments are comparable and repeatable.

2.1.2. *Relative humidity*

In this study, bubble method was developed and applied to regulate the chamber RH. Specifically, the clean air flow (RH < 5%) with 2 L/min was passing through a bottle with deionized water, and then the outlet flow (RH ~90%) was continuously injected into the chamber. This humidification process was easy to setup, without bringing particles or droplets into the chamber. Appendix A Fig. S2 shows the variation of RH and absolute water content (AWC) from two humidification tests. The AWC was calculated from temperature and RH measurement. The RH increased up to 80% after 4–5 hr, thus the experiments conducted under high RH conditions would be possible.

2.1.3. *Light spectrum and intensity*

Photolysis reactions are important because these reactions can initiate photochemistry and radical recycling. There are a variety of trace gases could be photolyzed, including NO_2, O_3, HCHO, CH_3CHO, HONO, NO_3, H_2O_2, etc. The chemical mechanism provided absorption cross sections and quantum yields used for the photolysis reactions. Blacklights are widely used as the typical light sources for indoor chambers. The measured light spectrum is shown in Appendix A Fig. S3a, peaked at ~365 nm with narrow range of 340–400 nm, which was also named as blue blacklight. The light spectrum was used as the input for mechanism modelling, as the quantum yields for products resulting from different photolysis species can be wavelength-dependent.

The equivalent light intensity (or photolysis rate, J_{NO2}) was determined by occasional NO_2 actinometry experiments (experiment number of ZJU076, ZJU206 and ZJU210). Specifically, a certain amount of NO_2 was injected into the chamber, and selected number of UV lights were turned on after NO_2 was stabilized and well mixed. Immediately, NO_2 would be photolyzed into NO and O_3, and NO-NO_2-O_3 went into equilibrium state, which were described as Reactions (1) – (3).

$$NO_2 + h\nu(\lambda < 400\ \text{nm}) \rightarrow NO + O(^3P) \quad (1)$$

$$O(^3P) + O_2 \rightarrow O_3 \quad (2)$$

$$O_3 + NO \rightarrow NO_2 + O_2 \quad (3)$$

According to Jeffries et al. (1975), J_{NO2} was calculated as following formula:

$$J_{NO2} = k_{NO+O_3}\frac{[O_3][NO]}{[NO_2]} \quad (4)$$

where k_{NO+O3} is the reaction rate constant of NO and O_3 (Atkinson et al., 2004), and $k_{NO+O3} = 1.4 \times 10^{-12} \times e^{-1310/T}$ cm^3/(molecule·sec).

From these experiments, their equivalent intensity values were determined using the measured photolysis rate of NO_2 (J_{NO2}), which are shown in Appendix A Fig. S3b. Note that 32 UV lamps were used before run number ZJU210, and 38 UV lamps were used after ZJU210, which could maintain the J_{NO2} within the range of 0.35–0.4 min^{-1} for later runs. We did not use 60 UV lambs because the temperature inside the chamber would increase up to 45°C, which is relatively high for normal experimental run. Obviously, the light intensity decay as run number increased, which was the normal case for UV lights. Therefore, we applied a fitted slope (the slope between J_{NO2} and run number) of −0.00044 min^{-1}, and the fitted J_{NO2} line (our best estimate) was assigned to each experiment run for mechanism modelling purpose, which could minimize the model input error of J_{NO2} due to run-to-run difference. In addition, J_{NO2} (0.35–0.4 min^{-1}) used for our chamber was matched to that from the ambient environment. For example, the long-term measurement of J_{NO2} was recorded at a coastal site of Greece during 2002-2006 (Gerasopoulos et al., 2012), with 5-year averaged J_{NO2} (referred to local noon time) ranging between 0.27 and 0.54 min^{-1}.

2.1.4. *Injection and mixing*

The gases injection panel was used to connect gas cylinders and chamber with mass flow controller. Once the injection was done, we need to make sure that the injected gases were well mixed and their concentrations were stabilized in the chamber before lights on. Most chambers consider to install a mixing fan inside the chamber, however, this may result in potential contamination or leak for the chamber. Here we followed the experimental injection procedure similar as CSIRO chamber (Li et al., 2018; White et al., 2018). Specifically, after

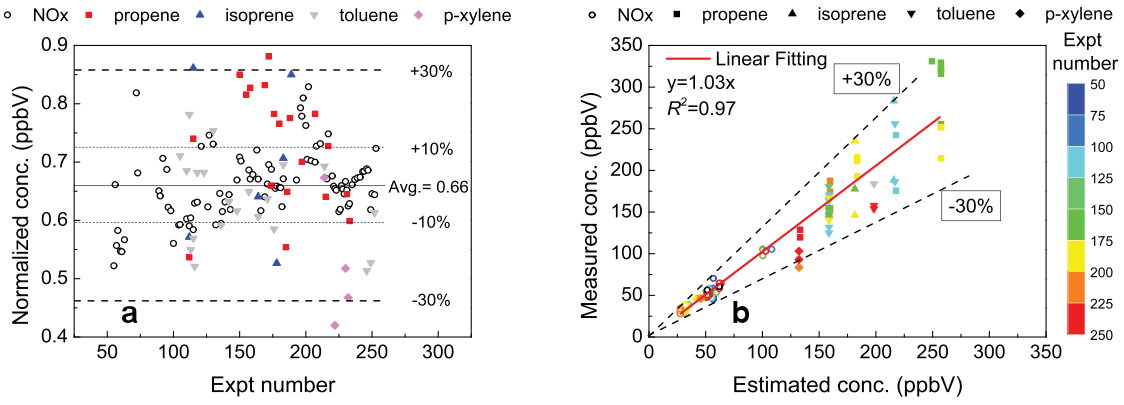

Fig. 2 – (a) Normalized NO_x and VOCs concentration of all experiments available (n = 147 for NO_x; n = 51 for VOCs); (b) Estimated vs. measured NO_x and VOCs concentrations colored by run number.

the injection was done, the chamber air was disturbed with high flow rate (~100 L/min) of clean air with short-term flush (<1 sec) for 5–10 times. As shown in Appendix A Fig. S4, there were 4 injections of NO and NO_2, and their concentrations stabilized within 20–30 min, which indicated that the gases were well mixed in the chamber.

In order to test the run-to-run injection variability, we introducted the concept of normalized concentration, which means the concentration in the chamber after injecting 1 sec at 1 L/min injection flow rate. It is defined as below in Eq. (5), and considering different flow rate and injection duration of gases used for each experiment.

$$C_{i,normalized} = \frac{C_{i,measured}}{F \times t} \quad (5)$$

where $C_{i,normalized}$ (ppbV) was the normalized concentration of compound i; $C_{i,measured}$ (ppbV) was the measured initial concentration of compound i; F was the flow rate of mass flow controller used for the gases injection, and usually set as 1 or 2 L/min; t (sec) was the injection duration.

For different experiments, the normalized concentration should be stable within experimental error range. The slight variation of the normalized concentration is reasonable because of the uncertainty from the chamber volume, injecting operation or measurement uncertainties. Fig. 2a shows the normalized NO_x and VOCs concentration against chamber run number, which was derived from the whole CAPS-ZJU dataset. The averaged normalized NO_x concentration was 0.66 ± 0.06 ppbV (n = 147), and over 90% of runs were within ±10% variation. The averaged normalized concentration of four VOC compounds were 0.66 ± 0.11 ppbV (n = 51), and showed larger bias than NO_x. The uncertaintiy of normalized VOCs concentrations was mostly within ±30%, which was primarily due to quantification uncertainties for VOC measurement.

According to the injection amount into the chamber, the initial concentration of NO_x and VOCs can be estimated. Fig. 2b shows the estimated versus measured NO_x and VOCs for all runs, which indicated reasonably good consistency (slope = 1.03, R^2 = 0.97). This suggested that the injection method we applied for CAPS-ZJU chamber was reliable to some extent, and the initial concentration of a given compound could be estimated with high confidence based on the injecting information (e.g., injection amount). Therefore, we applied this method to estimate the initial concentration of VOCs, which was listed in Appendix A Table S1.

2.1.5. *Gases wall loss*

Although Teflon-FEP material has good chemical inert, however, it is inevitable that gases and particles may deposit or absorb into the wall, which is known as chamber wall loss effect. The wall loss reaction can be regarded as first-order reaction, and the reaction rate could be obtained through monitoring the decay process of a given compound under dark conditions. As shown in Appendix A Fig. S5, the wall loss rate for O_3 and NO_2 were 4.97 × 10^{-4} and 1.67 × 10^{-5} min^{-1}, respectively. Table 1 also summarized the wall loss rates from different chamber facilities with various sizes over the world, and the gases wall loss rates characterized from CAPS-ZJU chamber were relatively low or comparable to other chambers.

2.1.6. *Particle wall loss*

Similar to gases wall loss, the particle wall loss could be regarded as first-order reaction. However, the particle wall loss rate is size-dependent, thus the particle wall loss rate for each size bin could be derived through the equation below:

$$\frac{dN(D_p)}{dt} = -k_{dep}(D_p) \times N(D_p) \quad (6)$$

where N (D_p) and k_{dep} (D_p) are the particle number concentration and particle wall loss rate at size bin D_p, respectively.

It should be noted that the size-dependent particle wall loss rate could be varied from aerosol composition and initial concentration. Thus, four wall loss tests were conducted using ammonium sulfate (AS) as seed particle with initial particle number concentration of 3.6 × 10^4 – 1.3 × 10^5 #/cm^3. In addition, one toluene/NO_x experiment (ZJU095) was selected to generate aged SOA in the chamber, and monitored the size evolution of aged SOA under dark condition after photooxidation ended. The merged results were summarized in Fig. 3a, and the best fitting curve for size-dependent particle wall loss rate was obtained through the equation (Takekawa et al., 2003; Wu et al., 2007) below:

$$k_{dep}(D_p) = a \times D_p^b + c \times D_p^d \quad (7)$$

where a, b, c and d are fitting parameters

In addition, Appendix A Table S3 summarized the fitting parameters of wall loss curves among different chamber facilities, and Fig. 3b compared these curves. In general, the particle wall loss rate of CAPS-ZJU chamber was 0.02–0.15 hr^{-1} within 70–400 nm, corresponding to half-life of 5–30 hr, which suggested that the aerosol wall loss for our chamber was not significant given a normal experiment time window of 6–8 hr.

2.2. *SAPRC gas-phase chemical mechanism evaluation*

2.2.1. *Wall mechanism setup and optimization*

It is critical to understand the impact of reactor walls on gas-phase chemistry, as they cannot be entirely negligible.

Table 1 – Summary of wall loss rates of different chamber facilities.

Chamber	Volume (m^3)	S/V (m^{-1})	NO_2 ($\times 10^{-4}$ min^{-1})	O_3 ($\times 10^{-4}$ min^{-1})	PM (hr^{-1})	Reference
ICCAS-DRC (right)	5	3.6	4.5	3.1	0.14–0.26	Wang et al., 2015
ICCAS-DRC (left)	5	3.6	3.8	2.5	0.12–0.21	Wang et al., 2015
GIG-CAS	30	2.1	1.39	1.31	0.10–0.41	Wang et al., 2014
PSI	27	2.0	0.32	2.4	/	Metzger et al., 2008
EUPHORE	200	0.65	6.9	1.8	/	Bloss et al., 2005
CSIRO	24.7	2.2	0.41	0.42	0.02–0.25	White et al., 2018
CAPS-ZJU	3	4.2	0.167	4.97	0.02–0.30	This work

S/V: surface to volume ratio; PM: wall loss rates in particle size range of 50–400 nm.

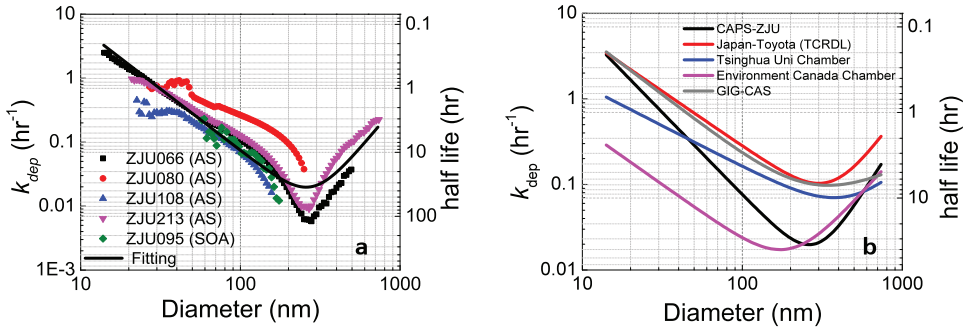

Fig. 3 – (a) Experimental and fitted curve from aerosol wall loss test experiments; (b) Comparison of wall loss fitting curve with other chambers. The parameterizations of the fitting curve are summarized in Appendix A Table S3.

Table 2 – CAPS-ZJU (this work) and CSIRO chamber (White et al., 2018) auxiliary wall mechanism determined for SAPRC mechanism.

Rate	CAPS-ZJU chamber	CSIRO chamber
Wall → HONO	$1.2 \times 10^{-5} \times J_{NO2}$	$1.3 \times 10^{-6} \times J_{NO2}$
Wall → HCHO	$5.0 \times 10^{-6} \times J_{NO2}$	$3.0 \times 10^{-5} \times J_{NO2}$
$[HONO]_i$[a]	1×10^{-2} ppbV	1×10^{-2} ppbV
NO_2 → Wall + YHONO × HONO	1.67×10^{-5} min^{-1}	4.08×10^{-5} min^{-1}
YHONO[a]	0.5	0.5
O_3 → Wall	4.97×10^{-4} min^{-1}	4.2×10^{-5} min^{-1}
N_2O_5 → Wall[a]	2.8×10^{-3} min^{-1}	2.8×10^{-3} min^{-1}
$N_2O_5 + H_2O$ → Wall[a]	1.5×10^{-6} $(ppmV \cdot min)^{-1}$	1.5×10^{-6} $(ppmV \cdot min)^{-1}$
OH → HO_2	10 min^{-1}	100 min^{-1}
HNO_3 → Wall[a]	1.98×10^{-4} min^{-1}	1.98×10^{-4} min^{-1}

[a] These parameters were same with CSIRO chamber, which were recommended values from SAPRC report.

For mechanism evaluation, background offgasing of NO_x and other reactive species (e.g., HCHO) are the most important factors. The NO_x offgasing can be represented in the model as inputs of any species that rapidly forms NO_x in atmospheric irradiation systems, such as NO, NO_2 and HONO. According to the method mentioned in previous literature (Carter et al., 2005), the HONO offgasing rate was determined indirectly by conducting model simulations of the appropriate characterization experiments (e.g., CO-NO_x and pure air experiments) to determine which parameter values best fit the data.

Table 2 summarized the CAPS-ZJU auxiliary wall mechanism determined for SAPRC mechanism. The wall loss rates of O_3 and NO_2 were determined from wall loss test experiments, which was described in Section 2.1.5. The HONO offgasing rate (wall → HONO) was tweaked and optimized with best fit from mechanism modelling of CO-NO_x and pure air experiments. The HONO offgasing rate was about one order higher than that from CSIRO chamber ($1.2 \times 10^{-5} \times J_{NO2}$ vs $1.3 \times 10^{-6} \times J_{NO2}$), and the estimated uncertainty of this parameter was abount ± 50% through the optimizing process. The reaction rate (OH → HO_2) was determined from the pure air experiments, which represented the reactivity of VOC from background air, but this rate was not sensitive and did not significantly affect model simulations for typical VOC-NO_x runs.

In addition, Δ(O_3-NO) is widely used as an indicator of the sum of O_3 formation and NO consumption (Carter and Heo, 2013; Azzi et al., 2010; Yarwood et al., 2010), which is described as below:

$$\Delta(O_3 - NO)_t = (O_3 - NO)_t - (O_3 - NO)_0 \quad (8)$$

Appendix A Fig. S6 showed the chamber data and SAPRC-11 modelled results of Δ(O_3-NO), O_3, NO, and NO_2 for CO-NO_x and pure air characterization experiments. In the SAPRC-11 mechanism model, we adapted two different auxiliary wall mech-

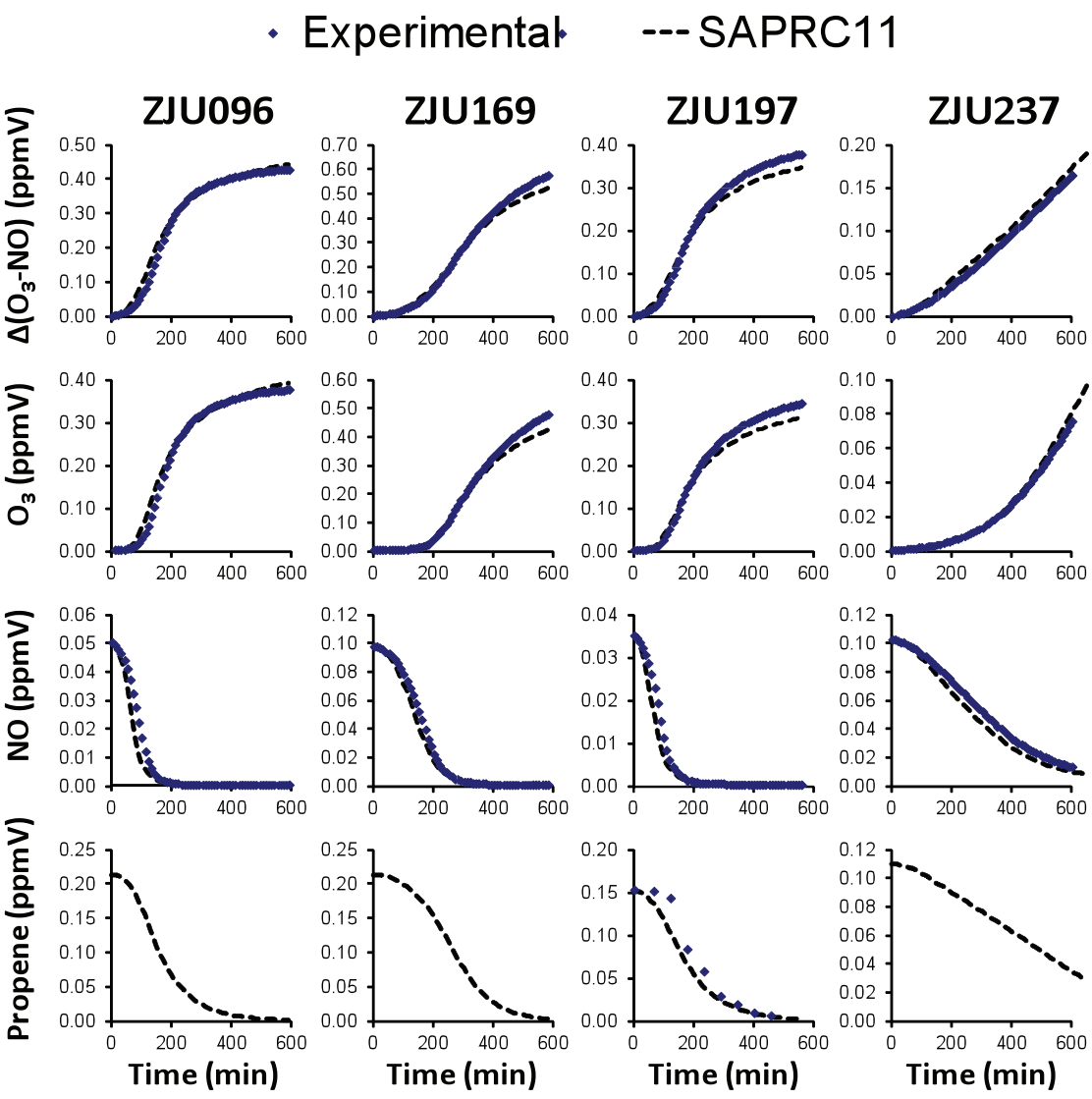

Fig. 4 – Δ(O_3 – NO), O_3, NO and propene predictions for SAPRC-11 against selected propene/NO_x experiments.

anisms for comparison. One for CAPS-ZJU chamber, and another one for CSIRO chamber, which were described in Table 2. It can be seen that the SAPRC-11 (adapted CAPS-ZJU auxiliary mechanism) agreed reasonably well with NO oxidation and O_3 formation rates, suggesting that the wall mechanism for CAPS-ZJU chamber was well established and optimized.

2.2.2. *Propene/NO_x photo-oxidation*

Propene/NO_x experiments have been frequently used to determine the ability of a smog chamber for chemical mechanism evaluation, due to the simple and well understood chemical mechanism of propene. The major reaction products of propene with OH are formaldehyde and acetaldehyde, and propene is also very reactive with a high ozone formation potential (Atkinson, 2000). As described in Appendix A Table S1, there were 40 propene/NO_x experiments being undertaken at CAPS-ZJU chamber, which covered a wide range of initial concentrations. The initial propene was ranged between 110 and 220 ppbV, while the initial NO_x was ranged between 20 and 110 ppbV. Fig. 4 and Appendix A Fig. S7 showed experimental data and SAPRC-11 modelled results for all propene/NO_x runs. For most of the experiments, it can been seen that the modelled results were reasonably good in predicting the O_3 formation and NO oxidation. Note that besides the initial VOC and NO_x concentrations were used as model input, the assigned photolysis rates (see details from Section 2.1.3) and the measured temperatures variation profiles of each experiment were also used as model input.

We used Δ(O_3-NO) as an indicator to assess the model error for mechanism predictions, which was defined as below:

$$\Delta(O_3 - NO)_{error} = \frac{\Delta(O_3 - NO)_{model} - \Delta(O_3 - NO)_{expt}}{\Delta(O_3 - NO)_{expt}} \quad (9)$$

Fig. 5a showed the time-dependent Δ(O_3 – NO) model error, and the model error and standard deviation were significant higher at the first 2 hr after the reaction was initiated. This indicated that the SAPRC-11 mechanism over-predicted Δ(O_3 – NO) by 20%–30% in average at initial stage. As the reaction went through after 4 hr, the averaged Δ(O_3 – NO) model error went down to −3% ± 7%. This phenomenon suggests that the mechanism still has some limitations at the staring period of photochemistry, in particular when O_3 is formed rapidly, as the fast HO_2 and RO_2 radical recycling processing has not yet been well understood in the current gas-phase chemistry.

The 6 hr Δ (O_3 – NO) was calculated at the specific time point at 6 hr, and Fig. 5b showed the 6 hr Δ (O_3 – NO) model er-

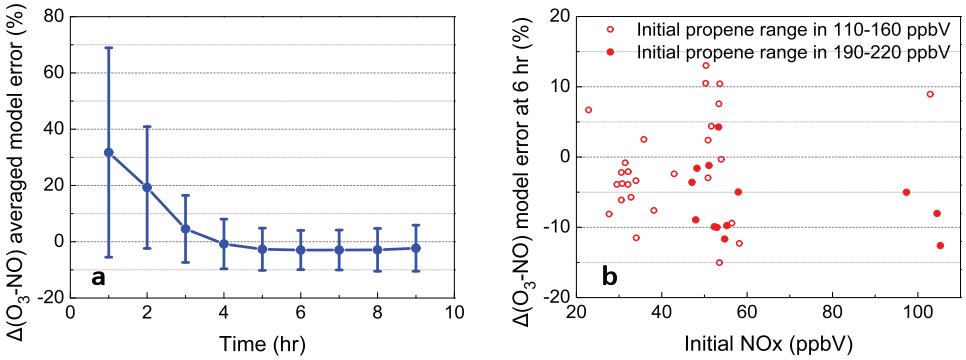

Fig. 5 – (a) Time-dependent averaged Δ(O_3 – NO) model error (avg. ± 1σ) obtained from 40 propene/NO_x experiments; (b) 6 hr Δ (O_3 – NO) model error for propene experiments against different initial conditions.

ror under various initial conditions. Overall, 34 out of 40 experiments showed 6 hr Δ (O_3 – NO) model error within ±10%. The initial propene concentrations were categorized into two subsets: 110–160 and 190–220 ppbV. However, no significant connection was found between model error and initial conditions. This suggested that the SAPRC-11 can give reasonably good predictions for propene-NO_x experiments under various initial concentrations, and also implied that CAPS-ZJU chamber was well characterized as the chamber data was reasonable for chemical mechanism evaluation.

2.2.3. *Isoprene/NO_x photo-oxidation*

Three isoprene experiments were carried out at CAPS-ZJU smog chamber. The initial conditions were similar among the three experiments, with initial isoprene of ~165 ppbV and initial NO_x of ~30 ppbV. Appendix A Fig. S8 showed the experimental data and SAPRC-11 modelled results for isoprene experiments. Obviously, the O_3 formation rate and final O_3 concentration were underestimated by SAPRC-11. However, the NO and isoprene decay process were accurately captured by the mechanism model, with NO and isoprene fully consumed at ~200 and ~500 min, respectively. Similar phenomenon was observed in our previous mechanism review for SAPRC-07 using CSIRO chamber data (Azzi et al., 2010), where the final O_3 predicted by SAPRC-07 was approximately 20% lower than observed values for all isoprene experiments. It should be noted that SAPRC-07 and SAPRC-11 has no difference on isoprene chemistry, as SAPRC-11 only updated aromatic chemistry from earlier version (Carter and Heo, 2013).

2.2.4. *Toluene/NO_x photo-oxidation*

Four experiments were performed using toluene and NO_x. The initial toluene varied from 140 to 180 ppbV, and initial NO_x varied from 30 to 60 ppbV, with VOC/NO_x (ppbC/ppbV, ppbC referred to carbon number volume concentration) ranged from 19.6 to 35.7. Appendix A Fig. S9 showed the experimental data as well as SAPRC-07 and SAPRC-11 modelled results for toluene experiments. There was a clear improvement in mechanism performance between SAPRC-11 and SAPRC-07 for the experiments evaluated, in particular to the O_3 formation rate and NO oxidation. This is consistent with the results from Carter and Heo (2013), which showed similar improvements compared to results for toluene experiments in this concentration range. Note that the toluene decay rate was underestimated by SAPRC-11 as observed in ZJU235, and this phenomenon was attributed to the underestimated OH radical by the current chemical mechanism, which reflected the limitation of the mechanism.

As shown in Fig. 6, by comparing the Δ(O_3 – NO) model error for both SAPRC-07 and SAPRC-11, some improvements were observed for 3 hr Δ(O_3 – NO) model error with later mechanism. Apart from this, both mechanisms were performed reasonably well at 6 hr across VOC/NO_x (ppbC/ppbV) range of 19.6–35.7, with Δ(O_3 – NO) model error within ±10%.

2.2.5. *p-Xylene/NO_x photo-oxidation*

Three *p*-xylene experiments were carried out at similar initial conditions, with initial *p*-xylene of ~110 ppbV and initial NO_x of ~50 ppbV. Appendix A Fig. S10 showed the experimental data as well as SAPRC-07 and SAPRC-11 modelled results for *p*-xylene experiments. Similar as observed in toluene experiments, *p*-xylene experiments also showed significantly improvement for O_3 prediction from SAPRC-11 mechanism compared to SAPRC-07, which was consistent with the results from Carter and Heo (2013) as the SAPRC-11 updated the aromatic chemistry. However, SAPRC-11 slightly over-predicted the NO oxidation rate, as the observed NO decay process was overall within the both mechanism prediction range. In addition, as observed in ZJU222 and ZJU232, *p*-xylene decay process was still under-predicted by SAPRC-11, with similar reasons for toluene.

Comparison of the calculated Δ(O_3 – NO) model errors at 3 and 6 hr is shown in Fig. 6. The VOC/NO_x (ppbC/ppbV) of the three *p*-xylene experiments was around ~17. Both Δ(O_3 – NO) model errors at 3 and 6 hr are largely improved within ±10% for the SAPRC-11. Specifically, 3 hr Δ(O_3 – NO) model errors improved from −51% ± 2% to 4% ± 4% (SAPRC-07 vs. SAPRC-11), and 6 hr Δ(O_3 – NO) model errors improved from −20% ± 4% to −4% ± 4%.

2.2.6. *Model sensitivity analysis*

A model sensitivity test was undertaken for four selected experiments for each hydrocarbon used in this study. The wall loss rates or parameters were varied by ± 50%, reflecting the large possible uncertainties in the estimation of these from the characterization experiments. In contrast, the initial experimental conditions or light intensity were varied by only ± 10%, which was considered a reasonable estimate of the upper and lower limit of the uncertainty of these parameters, as these parameters were determined from critical measurements.

Fig. 7 showed the sensitivity test undertaken for each species. Generally, it was determined that the largest uncertainties in model predictions were due to uncertainties in specific experimental conditions, such as the initial concentrations of reactants or the light intensity determined, which played a more dominant role than these wall loss parameters. However, HONO offgasing rate and O_3 wall loss rate were identified as the most important parameters among all these auxiliary mechanism parameters, which needs more careful characterization when performing the chemical mechanism

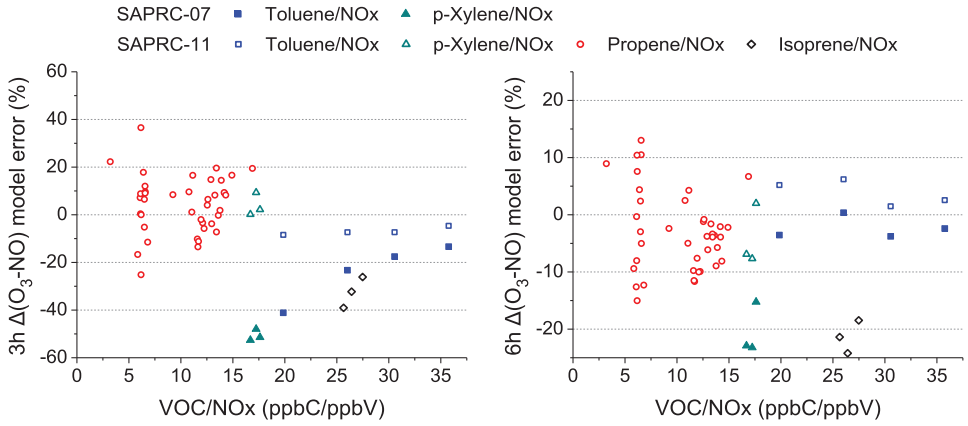

Fig. 6 – Δ(O_3 – NO) model error for propene, isoprene, toluene and *p*-xylene experiments at (a) 3 hr and (b) 6 hr.

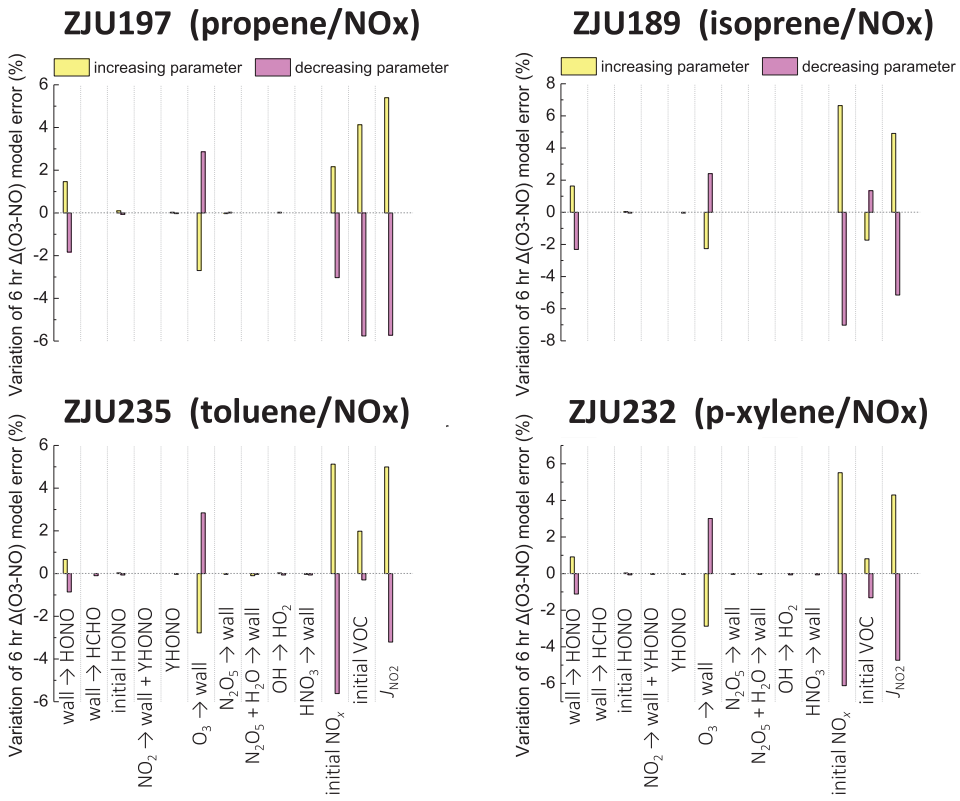

Fig. 7 – Variation in 6 hr Δ(O_3 – NO) model error for four selected experiment, with ±50% variation in wall parameters, and ±10% variation in initial conditions of NO_x, VOC, and J_{NO2}.

evaluation. Although the relative importance of these parameters identified may vary from run-to-run and chamber-to-chamber, the general conclusion could also be applied to the mechanism evaluation work by other chambers.

3. Conclusions

In this study, we developed a new smog chamber facility (CAPS-ZJU) to evaluate SAPRC gas-phase chemical mechanism. The chamber has been characterized in detail through a series of characterization experiments, including temperature variation profile, light spectrum and equivalent intensity (J_{NO2}), injection and mixing performance, as well as gases and particle wall loss. For example, the chamber air can be well mixed through "pulse flushing" within 20–30 min after injection, without introducing internal fan. In addition, the initial gases concentration can be reasonably inferred through the injection amount, which could provide confidence as model input for chemical mechanism evaluation, in particular when measurements are not available. The characterization results showed that our experimental protocols are reliable, which could provide more precise data for mechanism evaluation.

Most of the wall reaction rates were obtained through gases wall loss, CO-NO_x and pure air experiments, and other wall parameters were extracted largely from previous literatures for consistency, and eventually the auxiliary wall mechanism for

CAPS-ZJU chamber was setup and examined. Fifty chamber experiments were performed using propene, isoprene, toluene and *p*-xylene in the presence of NO_x for various initial concentrations. It was found that the SAPRC-11 can well predict the O_3 formation and NO oxidation for almost all propene runs, with 6 hr $\Delta(O_3 - NO)$ model error of –3% ± 7%, while the final O_3 was underestimated by ~20% for isoprene experiments. As for toluene and *p*-xylene experiments, it was confirmed that SAPRC-11 has significant improvement on aromatic chemistry than earlier version (SAPRC-07). The model sensitivity test showed that the initial concentrations of reactants and the light intensity as well as HONO offgasing rate and O_3 wall loss rate are the most sensitive values for model input, which needs to be carefully treated. All the experiments showed reasonably acceptable results against SAPRC mechanism modelling prediction, which also suggested that the CAPS-ZJU chamber data has the potential to evaluate other chemical mechanisms (e.g., CB, RACM, MCM) in the future.

Considering the heavily-equipped instrumentation, CAPS-ZJU smog chamber also has great potential on studying secondary aerosol formation, in particular under high RH conditions, which is largely driven through gas-phase or multiphase chemistry but not well understood yet. From this perspective, some chamber experiments target on aerosol physicochemical characterization or under high RH conditions are currently in progressing or planned, and will be discussed in subsequent papers.

Declaration of competing interest

The authors declared that they have no conflicts of interest to this work.

Acknowledgments

This work was supported by the Natural Science Foundation of China (No. 51876190), the Environmental Protection Agency of Hangzhou (No. 2017-008), the Innovative Research Groups of the National Natural Science Foundation of China (No. 51621005), and the program of Introducing Talents of Discipline to University (No. B08026). We thank Mr. Chunshan Liu of Beijing Convenient Environmental Tech Co. Ltd (http://www.bjkwnt.com/) for their help and support in smog chamber setup.

Appendix A. Supplementary data

Supplementary material associated with this article can be found in the online version at doi:10.1016/j.jes.2020.03.028.

REFERENCES

Atkinson, R., 2000. Atmospheric chemistry of VOCs and NOx. Atmos. Environ. 34 (12-14), 2063–2101.

Atkinson, R., Baulch, D.L., Cox, R.A., Crowley, J.N., Hampson, R.F., Hynes, R.G., et al., 2004. Evaluated kinetic and photochemical data for atmospheric chemistry: Volume I–gas phase reactions of Ox, HOx, NOx and SOx species. Atmos. Chem. Phys. 4 (6), 1461–1738.

Azzi, M., White, S.J., Angove, D.E., Jamie, I.M., Kaduewela, A., 2010. Evaluation of the SAPRC-07 mechanism against CSIRO smog chamber data. Atmos. Environ. 44 (14), 1707–1713.

Bloss, C., Wagner, V., Bonzanini, A., Jenkin, M.E., Wirtz, K., Martin-Reviejo, M., Pilling, M.J., 2005. Evaluation of detailed aromatic mechanisms (MCMv3 and MCMv3.1) against environmental chamber data. Atmos. Chem. Phys. 5 (3), 623–639.

Bonn, B., von Schneidemesser, E., Butler, T., Churkina, G., Ehlers, C., Grote, R., et al., 2018. Impact of vegetative emissions on urban ozone and biogenic secondary organic aerosol: Box model study for Berlin, Germany. J. Clean. Prod. 176, 827–841.

Boyd, C.M., Sanchez, J., Xu, L., Eugene, A.J., Nah, T., Tuet, W.Y., et al., 2015. Secondary organic aerosol (SOA) formation from the β-pinene + NO_3 system: effect of humidity and peroxy radical fate. Atmos. Chem. Phys. 15 (2), 7497–7522.

Carter, W.P., 2000. Implementation of the SAPRC-99 chemical mechanism into the Models-3 framework. In: Report to the United States Environmental Protection Agency, January 29.

Carter, W.P., 2010. Development of the SAPRC-07 chemical mechanism. Atmos. Environ. 44 (40), 5324–5335.

Carter, W.P., Heo, G., 2013. Development of revised SAPRC aromatics mechanisms. Atmos. Environ. 77, 404–414.

Carter, W.P.L., Cocker, D.R., Fitz, D.R., Malkina, I.L., Bumiller, K., Sauer, C.G., et al., 2005. A new environmental chamber for evaluation of gas-phase chemical mechanisms and secondary aerosol formation. Atmos. Environ. 39 (40), 7768–7788.

Chen, L., Bao, K., Li, K., Lv, B., Bao, Z., Lin, C., et al., 2017. Ozone and secondary organic aerosol formation of toluene/NOx irradiations under complex pollution scenarios. Aerosol Air Qual. Res. 17 (7), 1760–1771.

Gerasopoulos, E., Kazadzis, S., Vrekoussis, M., Kouvarakis, G., Liakakou, E., Kouremeti, N., et al., 2012. Factors affecting O_3 and NO_2 photolysis frequencies measured in the eastern Mediterranean during the five-year period 2002-2006. J. Geophys. Res. Atmos. 117 (D22), D22305.

Goliff, W.S., Stockwell, W.R., Lawson, C.V., 2013. The regional atmospheric chemistry mechanism, version 2. Atmos. Environ. 68, 174–185.

Hess, G.D., Carnovale, F., Cope, M.E., Johnson, G.M., 1992. The evaluation of some photochemical smog reaction mechanisms—I. Temperature and initial composition effects. Atmos. Environ. 26 (4), 625–641.

Hidy, G.M., 2019. Atmospheric chemistry in a box or a bag. Atmosphere-Basel 10 (7), 401.

Hildebrandt, L., Donahue, N.M., Pandis, S.N., 2009. High formation of secondary organic aerosol from the photo-oxidation of toluene. Atmos. Chem. Phys. 9 (9), 2973–2986.

Hynes, R.G., Saunders, D.E.A.M., Haverd, V., Azzi, M., 2005. Evaluation of two MCM v3.1 alkene mechanisms using indoor environmental chamber data. Atmos. Environ. 39 (38), 7251–7262.

Jeffries, H., Fox, D., Kamens, R., 1975. Outdoor smog chamber studies: Effect of hydrocarbon reduction on nitrogen dioxide. In: Document No[R]. EPA-650/3-75-011. US Environmental Protection Agency.

Li, K., Chen, L., Han, K., Lv, B., Bao, K., Wu, X., et al., 2017a. Smog chamber study on aging of combustion soot in isoprene/SO_2/NOx system: Changes of mass, size, effective density, morphology and mixing state. Atmos. Res. 184, 139–148.

Li, K., Chen, L., White, S.J., Han, K., Lv, B., Bao, K., et al., 2017b. Effect of nitrogen oxides (NO and NO2) and toluene on SO2 photooxidation, nucleation and growth: A smog chamber study. Atmos. Res. 192, 38–47.

Li, K., Chen, L., White, S.J., Yu, H., Wu, X., Gao, X., et al., 2018. Smog chamber study of the role of NH3 in new particle formation from photo-oxidation of aromatic hydrocarbons. Sci. Total Environ. 619, 927–937.

Metzger, A., Dommen, J., Gaeggeler, K., Duplissy, J., 2008. Evaluation of 1,3,5 trimethylbenzene degradation in the detailed tropospheric chemistry mechanism, MCMv3.1, using environmental chamber data. Atmos. Chem. Phys. 8 (3), 11567–11607.

Ng, N.L., Kroll, J.H., Chan, A.W.H., Chhabra, P.S., 2007. Secondary organic aerosol formation from m-xylene, toluene, and benzene. Atmos. Chem. Phys. 7 (14), 3909–3922.

Seinfeld, J.H., Pandis, S.N., 2016. Atmospheric chemistry and physics: from air pollution to climate change. John Wiley and Sons.

Stockwell, W.R., Kirchner, F., Kuhn, M., Seefeld, S., 1997. A new mechanism for regional atmospheric chemistry modeling. J. Geophys. Res. Atmos. 102 (D22), 25847–25879.

Takekawa, H., Minoura, H., Yamazaki, S., 2003. Temperature dependence of secondary organic aerosol formation by photo-oxidation of hydrocarbons. Atmos. Environ. 37 (24), 3413–3424.

Venecek, M.A., Cai, C., Kaduwela, A., Avise, J., Carter, W.P.L., Kleeman, M.J., 2018. Analysis of SAPRC16 chemical mechanism for ambient simulations. Atmos. Environ. 192, 136–150.

Wang, W., Li, K., Zhou, L., Ge, M., Hou, S., Tong, S., et al., 2015. Evaluation and application of dual-reactor chamber for studying atmospheric oxidation processes and mechanisms. Acta Phys. -Chim. Sin. 31 (07), 1251–1259.

Wang, X., Liu, T., Bernard, F., Ding, X., Wen, S., Zhang, Y., et al., 2014. Design and characterization of a smog chamber for studying gas-phase chemical mechanisms and aerosol formation. Atmos. Meas. Tech. 7 (1), 301–313.

White, S., Angove, D., Li, K., Campbell, I., Element, A., Halliburton, B., et al., 2018. Development of a new smog chamber for studying the impact of different UV lamps on SAPRC chemical mechanism predictions and aerosol formation. Environ. Chem. 3 (15), 171–182.

Wu, S., Lv, Z., Hao, J., Zhao, Z., Li, J., Hideto, T., et al., 2007. Construction and characterization of an atmospheric simulation smog chamber. Adv. Atmos. Sci. 24 (2), 250–258.

Yarwood, G., Rao, S., Yocke, M.A., Whitten, G.Z., 2005. Updates to the carbon bond chemical mechanism: CB05. In: Final report to the US EPA, RT-04006758.

Yarwood, G., Whitten, G.Z., Jung, J., Heo, G., Allen, D.T., 2010. Development, Evaluation and Testing of Version 6 of the Carbon Bond Chemical Mechanism (CB6). In: Final Report to Texas Commission on Environmental Quality.